Valence-band electronic structure of ZnSe(001) thin films: Theory and experiment

L. Plucinski* and R. L. Johnson
Institut für Experimentalphysik, Universität Hamburg, Luruper Chaussee 149, D-22761, Hamburg, Germany

A. Fleszar and W. Hanke
Institut für Theoretische Physik, Universität Würzburg, Am Hubland, D-97074 Würzburg, Germany

W. Weigand and C. Kumpf
Experimentelle Physik II, Universität Würzburg, Am Hubland, D-97074 Würzburg, Germany

C. Heske
Department of Chemistry, University of Nevada, Las Vegas (UNLV) ,
4505 Maryland Parkway, Mail Stop 454003, Las Vegas, Nevada 89154, USA

E. Umbach
Experimentelle Physik II, Universität Würzburg, Am Hubland, D-97074 Würzburg, Germany

T. Schallenberg and L. W. Molenkamp
Experimentelle Physik III, Universität Würzburg, Am Hubland, D-97074 Würzburg, Germany
(Received 21 January 2004; published 15 September 2004)

Angle-resolved photoemission spectra of ZnSe(001) thin films have been measured using monochromatic vacuum-ultraviolet synchrotron radiation. The experimental width of the valence band at high symmetry points differs significantly from previously published data, but agrees well with our new *ab initio* band structure calculated including relativistic effects. Surface states were clearly identified by comparing the angle-resolved photoemission spectra with the surface electronic structure calculated for the ZnSe(001)-$c(2\times2)$ reconstruction.

DOI: 10.1103/PhysRevB.70.125308 PACS number(s): 79.60.Bm, 71.20.−b, 73.20.−r

I. INTRODUCTION

Zinc selenide is a wide band-gap semiconductor with a very low absorption coefficient for wavelengths between 0.63 μm to 18 μm. It is a key material in high-power infrared lasers and used for infrared windows, lenses, and prisms. Recent progress in fabricating ZnSe laser diodes for the blue-green and white spectral regions[1–3] has rekindled interest in the fundamental properties of this material. The successful photonics applications[4,5] motivated the present comprehensive investigation of the electronic structure of ZnSe(001) which combines experimental photoemission studies with state-of-the-art theoretical calculations.

Previous photoemission studies on MBE-grown ZnSe(001) samples have provided some important insights, but remain incomplete. For example, the recent experimental investigations of Dröge *et al.*[6] focused only on normal-emission photoelectron spectra. The earlier work of Zhang *et al.*[7] on the Se-rich (2×1) surface provided evidence for three surface resonances, and the publication by Xue *et al.*[8] emphasizes the experimental differences in the electronic structure between the Se-rich (2×1) and the $c(2\times2)$ Zn-terminated surfaces. To our knowledge no theoretical results on the surface electronic band structure of different reconstructions of ZnSe(001) have been published to date.

Angle-resolved photoelectron spectroscopy (ARPES) is widely used to determine the energy and momentum of the occupied electronic states in crystalline solids. In a photoemission experiment only the wave vector component parallel to the surface, $k_{\|}$, is conserved since the presence of the surface breaks the translational symmetry in the perpendicular direction; the momentum transfer of the photon can be neglected in the vacuum-ultraviolet (VUV) region. Within the direct transition model, $k_{\perp}$ can be determined by assuming appropriate final states. Either free-electron-like or calculated final states are frequently employed, and experimental techniques to establish the absolute crystal momentum have also been developed.[9] Here we present both experimental and theoretical results on the bulk and the $c(2\times2)$ surface electronic structure of ZnSe(001), calculated using density functional theory within the local density approximation (DFT-LDA). We are able to derive a detailed picture of the valence band electronic structure of ZnSe(001) by combining various approaches to interpret the angle-resolved photoemission data.

This paper is organized as follows: experimental details are presented in Sec. II and the theoretical calculations in Sec. III. The bulk electronic structure of ZnSe is described in Sec. IV and the surface electronic structure of ZnSe(001)-$c(2\times2)$ is discussed in Sec. V.

II. EXPERIMENT

High quality ZnSe(001) thin films were grown on GaAs(001) substrates using molecular beam epitaxy (MBE)

at Würzburg University. The samples were transfered under ultrahigh vacuum (UHV) from the growth chamber in Würzburg to the beamlines at the Hamburg Synchrotron Radiation Laboratory (HASYLAB) using a portable chamber developed for both x-ray[10] and photoemission investigations. The samples were passivated with a Se-cap for additional protection although the pressure in the transfer chamber was better than 5×10^{-9} mbar. The 0.27% lattice mismatch between the GaAs substrate and the epitaxial ZnSe film induces pseudomorphic strain. Since the critical thickness for this system is well above 100 nm (Ref. 11) the samples investigated here, with thicknesses 50–100 nm, were all pseudomorphically strained.

The experiments were performed at the Seya-Namioka monochromator beamline F2.2 at HASYLAB.[12] The results presented in this paper were obtained on the ZnSe(001)-$c(2\times2)$ reconstructed surface prepared by annealing to 450 °C as described by Chen *et al.*[13] The samples were oriented using low energy electron diffraction (LEED). During the measurements the pressure in the analyzer chamber was better than 1×10^{-10} mbar.

The momentum space was mapped in detail along the main symmetry directions in the Brillouin zone (BZ). The linearly polarized synchrotron light was incident at 45° to the sample normal and the polarization vector was in the plane defined by the direction of the incoming photons and the sample normal. The overall instrumental energy resolution was typically 100 meV, with an angular resolution of 2°.

III. THEORY

The bulk band structure of ZnSe was calculated using DFT-LDA with Zn^{12+} and Se^{6+} pseudopotentials including relativistic effects. The experimental lattice constant $a=5.67$ Å and a cutoff energy for the plane waves of 60 Ry were used. The band structure of the occupied valence bands is depicted in Fig. 1 and for comparison a representative normal emission spectrum recorded at $\hbar\omega=25$ eV is plotted on the left-hand side. Our calculations yield a fundamental gap of 0.81 eV which is far too small compared with the experimental value of 2.82 eV at 0 K (Ref. 14) but this is a well-known deficiency of LDA. The Zn 3*d* bands at Γ are calculated to lie between −6.68 and −7.19 eV, which is about 2 eV higher than the experimental binding energy. This is a further well-known problem of the local-density approximation and has been discussed in detail by Zhang *et al.*[15]

The lowest part of the valence band between −13.47 eV at Γ and −12.36 eV at *W* originates from Se 4*s* levels and the upper part from −5.55 eV at *L* to 0 eV at Γ has mainly Se 4*p* character. The uppermost part of the valence band consists of six electronic bands which form three doubly-degenerate bands in the Γ-*X* and Γ-*L* directions. In this paper (as in Ref. 16) we call the lower of the valence bands appearing at −5.10 eV at *X* the *sh* (split-off hole) band and the two upper bands appearing at −2.54 and −2.36 eV at *X* the *lh* (light hole) and *hh* (heavy hole) bands. Note that for the Γ-*K*-*X* direction the degeneracy is removed, but the splittings of the three bands are small so the nomenclature with *sh*, *lh*, and *hh* can still be used. Band structure calculations on ZnSe have been performed by many groups in the past. In Table I we compare our results for the eigenvalues of the valence bands in *X* and *L* to some of the published results.[17–20]

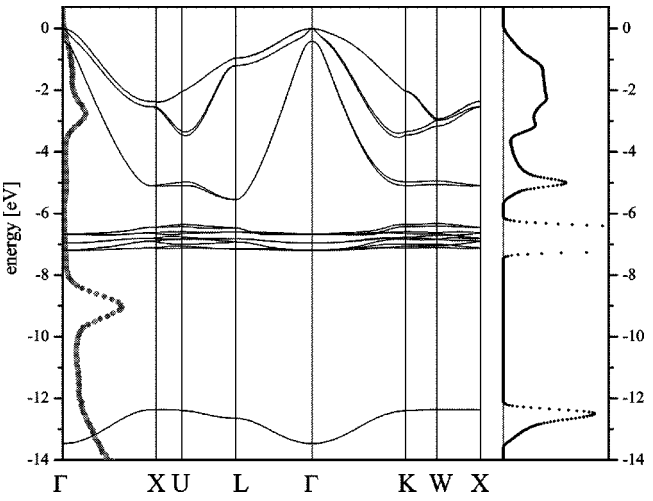

FIG. 1. Theoretical valence band structure of bulk ZnSe. The zero of the energy scale was adjusted to the VBM. On the left-hand side an experimental spectrum taken at normal emission with $\hbar\omega=25$ eV is shown for comparison, and the theoretical density of states (DOS) is depicted on the right-hand side.

The theoretical photocurrent was calculated using the Golden rule formalism by generalizing the formula given in Ref. 21 to arbitrary emission angles. The angle-resolved photoelectron energy spectrum at photon energy $\hbar\omega$, is

$$I(E,\hbar\omega,\vartheta)\propto\sum_{i,f}\int dk_{\parallel}\int dk_{\perp}\,\lambda_{\mathbf{k}_f}t_{\mathbf{k}_f}|\langle\psi_{\mathbf{k}i}|\mathbf{A}\cdot\mathbf{p}|\psi_{\mathbf{k}f}\rangle|^2 \times\delta(E_f(\mathbf{k})-E_i(\mathbf{k})-\hbar\omega)\,\delta(E-E_f(\mathbf{k}))\,\delta(\vartheta-\overline{\vartheta}), \quad (1)$$

where $\psi_{\mathbf{k}i}$, E_i and $\psi_{\mathbf{k}f}$, E_f are the Kohn-Sham wave functions

TABLE I. Eigenvalues of the *sh*, *lh*, and *hh* bands for ZnSe at *L* and *X* relative to the valence band maximum. The experimental values extracted from results presented in Secs. IV B and IV C are given. The *lh* and *hh* bands are not degenerate in our Zn^{12+} calculation.

Point	Ref. 17 Zn^{12+}	Ref. 18 Zn^{12+}	Ref. 18 Zn^{12+}	Ref. 19 GW	Ref. 20 GW	This work Zn^{2+}	This work Zn^{12+}	Experiment
L sh	−5.21	−4.39	−5.53	−5.23	−5.3	−5.16	−5.55	−5.4
X sh	−4.82	−4.24	−5.02	−5.03	−4.7	−4.94	−5.10	−5.1
X lh, hh	−2.20	−1.56	−2.39	−2.08	−2.2	−2.02	−2.36, −2.54	−2.6

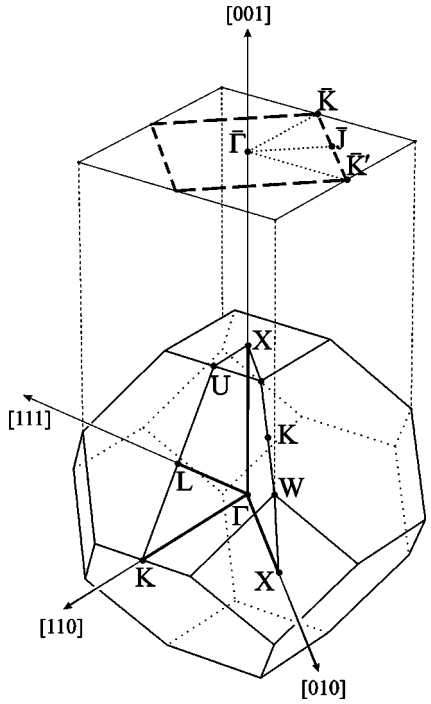

FIG. 2. Brillouin zone for zinc-blende lattice together with the related surface Brillouin zone for the (001) surface. The dashed line indicates the surface Brillouin zone for the $c(2\times2)$ reconstruction.

and energies of the bulk initial and final states. $I(E,\hbar\omega,\vartheta)$ is calculated as a function of the binding energy of the occupied states E, the incident photon energy $\hbar\omega$ and the polar angle ϑ. The polar angle of the outgoing electrons $\bar{\vartheta}$ is related to $\mathbf{k}_\parallel$ by $k_\parallel=\sqrt{(2m/\hbar^2)E_k}\sin\bar{\vartheta}$, $\lambda_{\mathbf{k}f}$ is the inelastic mean free path of excited electrons in the bulk. The quantity $t_{\mathbf{k}f}$ describes the transmission coefficient across the surface barrier for a final state $\psi_{\mathbf{k}f}$ and is calculated by projecting each bulk final state onto outgoing plane waves characterized by appropriate wave vectors.[21] The double integral in Eq. (1) was calculated using Lorentzians for the δ functions and a dense discrete mesh of $\mathbf{k}_\parallel$ and $k_\perp$ points.

The calculations of the surface electronic band structure of ZnSe(001)-$c(2\times2)$ were performed using the FHI98MD program package[22] with Zn^{2+} and Se^{6+} pseudopotentials—details are presented in Sec. V. The relationship between the bulk and surface Brillouin zones is shown in Fig. 2.

IV. BULK ELECTRONIC STRUCTURE

Photoemission experiments on solids in the VUV photon energy range are very surface sensitive due to the short mean free path of the photoelectrons (typically 0.5–2 nm) and hence the spectra contain both bulk- and surface-related features. The separation of bulk and surface features is a difficult task, and one of the best tests is to compare the experimental results to the calculated surface band structure. In the following we present a relatively complete picture of the bulk band structure of ZnSe(001) by interpreting the spectral features using in succession: (a) free-electron final-states, (b) a two-dimensional array of DFT-LDA final states, and (c) comparison with theoretical spectra.

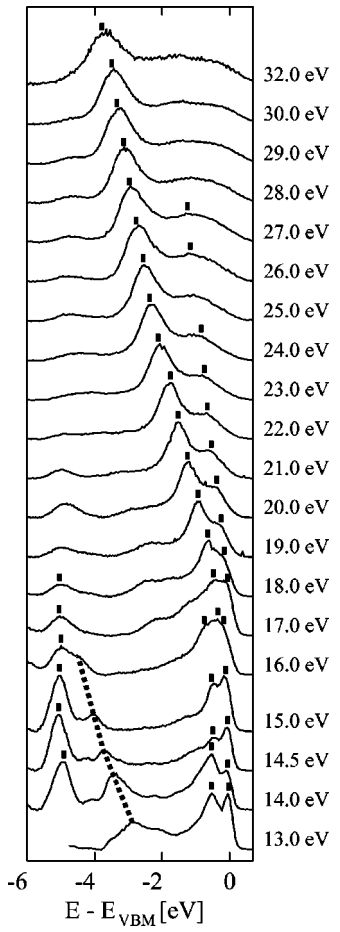

FIG. 3. Set of normal emission spectra measured on ZnSe(001). Bars indicate features taken into account for constructing the band structure. The dotted line indicates one of the dispersing features which could not be interpreted within the free-electron final state model.

A. Normal emission

When mapping the valence band electronic structure using ARPES with synchrotron light one first collects a set of normal emission spectra for the whole accessible photon energy range. Normal emission results are easiest to interpret and permit a strategy for subsequent off-normal scans to be defined. Figure 3 shows a set of normal emission spectra from ZnSe(001). The energy scale is relative to the valence band maximum (VBM). All spectra are background corrected and normalized. Peaks related to direct transitions were located using inverted second derivatives. The spectra in Fig. 3 are dominated by the dispersive peak related to the *sh* band for photon energies from $\hbar\omega=19$ to 32 eV. The fit to this peak is unambiguous. The less dispersive and less distinct features related to the *lh* and *hh* bands between −1.3 and 0 eV for $\hbar\omega$ from 17 to 27 eV and the spin-orbit split features near the Γ point for $\hbar\omega$ from 13 to 15 eV are marked. The decrease in the intensities of the *lh* and *hh*

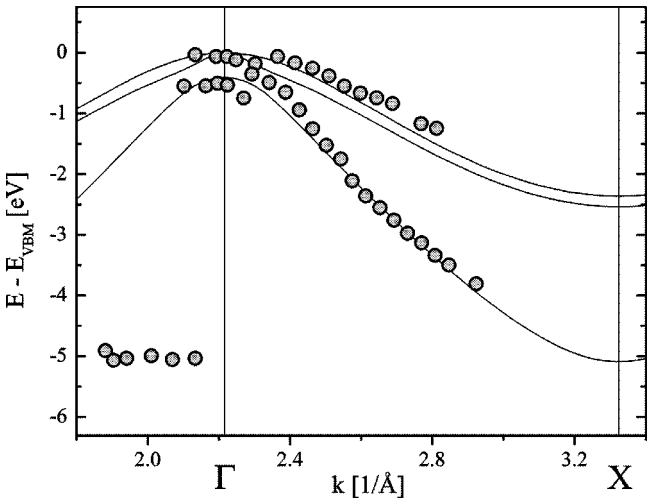

FIG. 4. Band structure along Γ-*X* constructed from the spectral features indicated in Fig. 3. Solid lines show the theoretical band structure.

bands with increasing photon energy can be explained using selection rule arguments.[23] The nondispersive features at −5 eV are discussed in Sec. IV C.

The features indicated in Fig. 3 were used to construct the band structure shown in Fig. 4 which also includes the results of the theoretical calculations. The wave vectors of the corresponding transitions were found using free-electron final-states with

$$k_{\perp} = \sqrt{\frac{2m}{\hbar^2}(E_k + V_0)}, \tag{2}$$

where E_k is the kinetic energy of the photoelectrons and the inner potential V_0 takes into account the potential barrier at the surface. When using free-electron final states V_0 is adjusted to give good agreement between the experimental and theoretical band structure. We found best agreement for $V_0 = 11.2$ eV and this value was used to construct the band structure in Fig. 4. There is good agreement between the calculation and the dispersion of the experimental features from Fig. 3. The experimental spin-orbit splitting of 0.40–0.45 eV at the Γ point is very close to the theoretical value of 0.41 eV.

There are more dispersive peaks in Fig. 3 than those marked with bars. The dotted line marks a dispersive feature that could not be explained within the free-electron final-state model. This feature is not an Auger transition because the kinetic energy is not constant.

In Fig. 5 we show experimental final-state bands on top of the free-electron parabolas and the DFT-LDA band structure. The unoccupied DFT-LDA bands were shifted to reproduce the experimental band gap. The experimental final-state bands were created on the assumption that the theoretical *sh* band is correct and the band indicated by the △ symbols was created from the dominant peak in the normal-emission EDCs. It can be seen that the symbols follow both the free-electron and the DFT-LDA bands, but a gap starts to open up in the region closer to Γ. The final-state band indicated by □

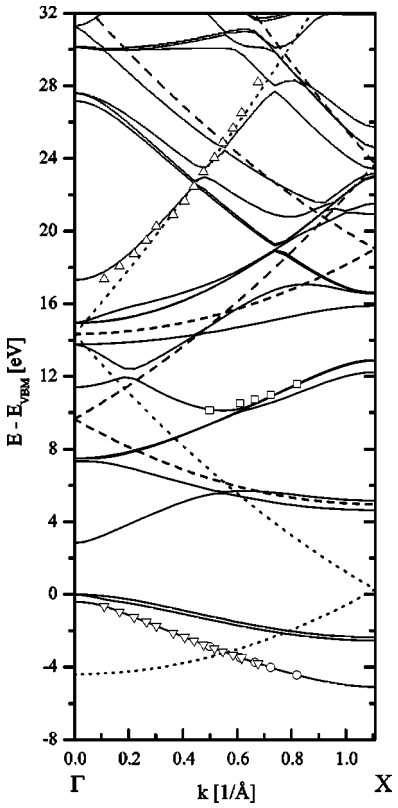

FIG. 5. Final state bands for bulk ZnSe along the Γ-*X* direction. The experimental final state bands are marked by △ and □ symbols and the ▽ and ○ symbols indicate the corresponding initial states. The primary-cone and secondary-cone free-electron parabolas are indicated by the dotted and dashed lines.

symbols was created from the features indicated by the dotted line in Fig. 3. This band is in agreement with the DFT-LDA calculation and there is no free-electron parabola (neither primary nor secondary cone) that could be assigned to it. This shows that for final-state energies in the lower region (below 20 eV) the free-electron model fails to explain some distinct features present in the EDCs. In spite of the known problems of the DFT-LDA method for excited states our conclusion is that the *scissors*-operator shifted array of DFT-LDA final states is in surprisingly good agreement with experiment for final-state energies up to about 24 eV. For energies above 28 eV the experimental results do not correspond to the DFT-LDA final states and the free-electron parabola gives better agreement.

B. Off-normal emission in the Γ*KWX* plane

Without a knowledge of both the initial and final state dispersions it is not possible to follow an arbitrarily defined path in the BZ in an off-normal ARPES experiment. However, one can maximize the probability that the momentum of the probed states is close to the desired one by assuming free-electron final states when choosing the photon energy and emission angle according to

$$k_{\parallel} = \sqrt{\frac{2m}{\hbar^2}E_k}\sin\vartheta,$$

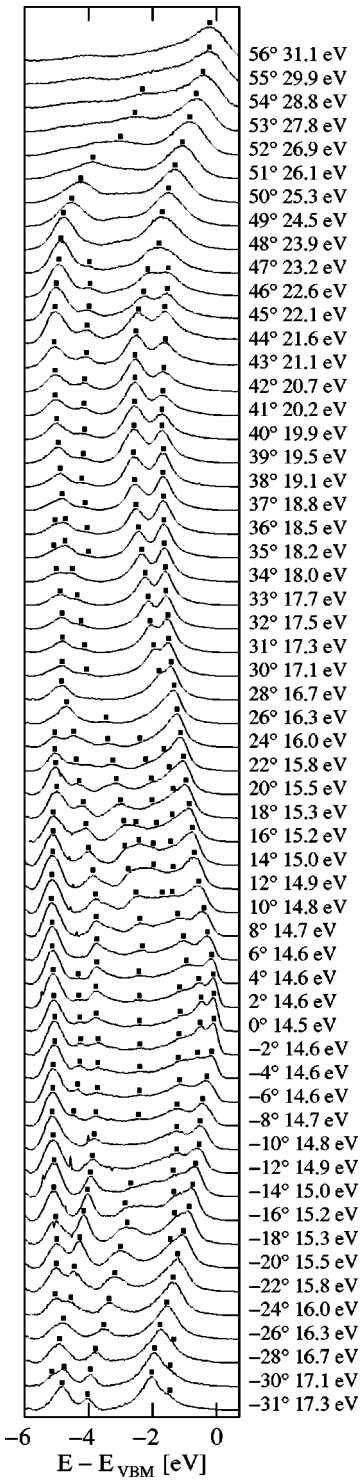

FIG. 6. Off-normal emission spectra in the Γ*KWX* plane from ZnSe(001). Dispersive spectral features are indicated by bars.

$$k_\perp = \sqrt{\frac{2m}{\hbar^2}(E_k \cos^2 \vartheta + V_0)}. \quad (3)$$

Here primary-cone direct transitions are considered, E_k and V_0 are defined as in Eq. (2), and ϑ is the polar angle of the emitted electrons with respect to the sample normal.

Figure 6 shows a set of off-normal spectra in the Γ*KWX* plane performed with small angular steps. In order to follow the Γ-*X* direction in the bulk BZ, the photon energies and detection angles were chosen using Eq. (3) with $V_0 = 11.2$ eV such that $k_\perp$ is kept constant for features appearing at the VBM. The scan was performed in the plane defined by the direction of the incoming photons and the surface normal. The spectra in Fig. 6 show several distinct dispersive features that could be easily identified and fitted. The band structure constructed from the features indicated in Fig. 6 is shown in Fig. 7 where the majority of the features (plotted as circles) can be ascribed to primary-cone bulk transitions, but there are also features marked by crosses that cannot be described in a simple way. As in the normal emission spectra the spin-orbit splitting is observed near the Γ point. The experimental and theoretically calculated spectra are compared in Fig. 8. The calculation of the theoretical spectra based on Eq. (1) gives only spectral features arising from the bulk band structure. The experimental data reveals two peaks that are clearly not present in the theoretical spectra which shows that they must be surface related. We will discuss these surface features in Sec. V.

At $\mathbf{k}_\parallel = (1,0,0) \times 2\pi/a$, related to the *X* point, we find that the *sh* band lies at −5.1 eV and *lh* and *hh* bands are at −2.6 eV (no splitting was observed experimentally). The value for the *sh* band can be assigned to the *X* point since, according to theory, at $\mathbf{k}_\parallel = (1,0,0) \times 2\pi/a$ only those bands from the *X*-*W* direction which lie in a narrow range between −5.1 and −4.95 eV are projected onto the surface. The value for the *lh* and *hh* bands may be less accurate due to a larger band width in the *X*-*W* direction and final-state effects.

C. Off-normal emission in Γ*KLUX* plane

We have performed a scan in the Γ*KLUX* plane assuming free-electron final states to select the appropriate photon energies and emission angles to map along the Γ-*K*-*X* [110] direction. This scan was performed in the plane perpendicular to the plane defined by the directions of the incoming photons and the surface normal.

Figure 9 shows the experimental band structure in the Γ*KLUX* plane, constructed assuming free-electron final states, plotted on top of the projected bulk band structure. In this figure one can see that the majority of the spectral features can be attributed to bulk states. Let us concentrate on the peak at the bottom of the valence band for *k* between 0.5 and 1 Å^{-1} indicated by the ▽ symbols. The corresponding spectra and their inverted second derivatives are shown in Fig. 10. The minimum of the band is at −5.4 eV which is 0.3 eV lower than the position of the *sh* band at *X* given in the preceding section. This band is related to emission from the *sh* band near the *L* point which is explained as a transition to non free-electron final-state since the spectra were collected in the Γ*KLUX* plane. The *L* point has the coordinates $2\pi/a(\frac{1}{2},\frac{1}{2},\frac{1}{2})$ and since $\mathbf{k}_\parallel$ is conserved in the photoemission process emission from *L* in the reduced zone scheme is only possible for $|\mathbf{k}_\parallel| = \sqrt{2}\pi/a \approx 0.78$ Å^{-1} which fits very well to the bottom of the band as can be seen in Fig. 9. If we assume free-electron final states and secondary-cone emission with a $\mathbf{G} = (2\pi/a)(-1,-1,-1)$ final state band we

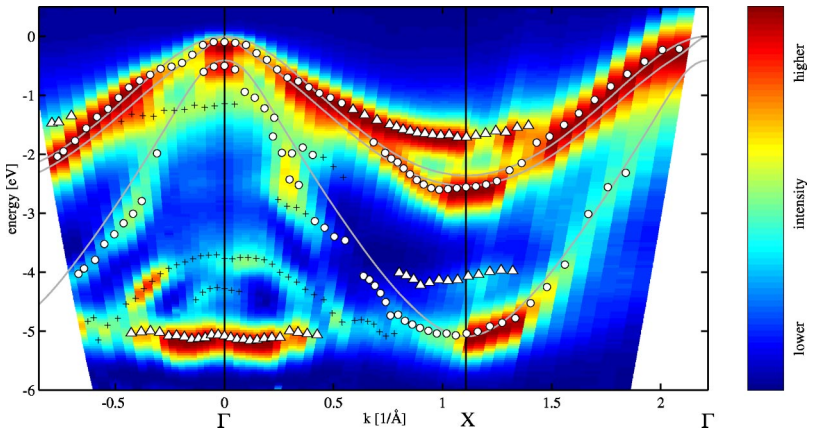

FIG. 7. (Color online) Band structure constructed using the features indicated in Fig. 6. Circles indicate primary-cone bulk related features, triangles indicate surface related features and the nondispersive feature at around −5 eV, and crosses indicate secondary-cone emissions or features related to final-state effects. Solid lines show the theoretical band structure along Γ-*X*. Color map areas represent the same spectra as in Fig. 6 but plotted in the $E(k)$ plane with k vectors calculated using Eq. (3).

find for the feature at −5.4 eV in the spectrum at $\hbar\omega = 19.5$ eV and 39°

$$k_\perp = \sqrt{(2m/\hbar^2)E - |\mathbf{k}_\parallel + \mathbf{G}_\parallel|^2} - \mathbf{G}_\perp \approx 0.12 \times (2\pi/a),$$

while primary-cone emission ($\mathbf{G}_\parallel = 0$) gives $k_\perp \approx 0.19 \times (2\pi/a)$, after reduction to the first BZ. Both of these **k** values are away from the *L* point. Thus the free-electron final state model fails to predict the discussed emission from the bottom of the *sh* band.

Olguín *et al.*[24] have presented an interpretation for the nondispersive features, which lie at energies ∼−5 eV, based on tight-binding calculations and a Green's function formalism assuming an unrelaxed, unreconstructed, ideal interface. It is apparent from Fig. 9 that these nondispersive features lie on the edge of the projected bulk band structure. In our interpretation they are transitions from the neighborhood of the

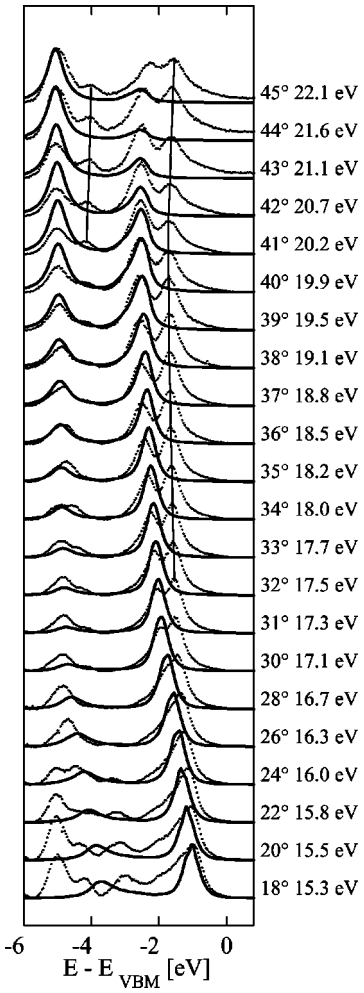

FIG. 8. Comparison of the experimental (dots) and theoretical (solid lines) spectra for off-normal emission in the Γ*KWX* plane. Surface related features are indicated by the guidelines. The experimental spectra are a selection from Fig. 6.

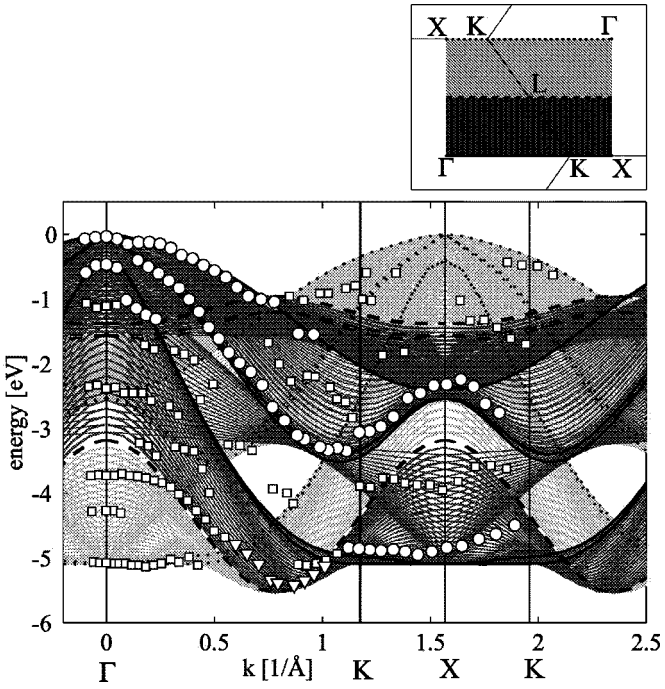

FIG. 9. The band structure for Γ*KLUX* plane constructed assuming free-electron final states. Circles show bulk-related primary-cone features. Squares and triangles indicate other dispersions that cannot be explained as primary-cone free-electron features. Darker gray areas show the projected bulk band structure for Γ*KLUX* plane for $\mathbf{k}_\perp$ from 0 to π/a and lighter gray areas for $\mathbf{k}_\perp$ from π/a to $2\pi/a$. Solid lines show bands in Γ*KLUX* plane at $\mathbf{k}_\perp = 0$ (along Γ-*K*-*X*), dashed lines for $\mathbf{k}_\perp = \pi/a$ (this includes *L* point), and dotted lines for $\mathbf{k}_\perp = 2\pi/a$ (along *X*-*K*-Γ). It is also schematically shown on the top-right of the figure in the BZ section. See the text for details.

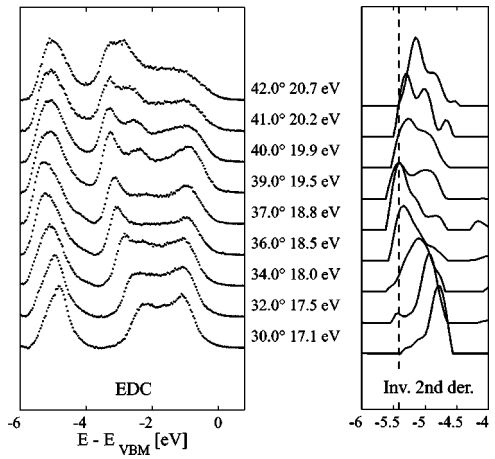

FIG. 10. Energy distribution curves for $\mathbf{k}_{\parallel} \simeq 0.5-1$ Å^{-1} in the $\Gamma KLUX$ plane and the corresponding inverted second derivatives near the valence band minimum. The vertical dashed line positioned at −5.4 eV indicates the valence band minimum.

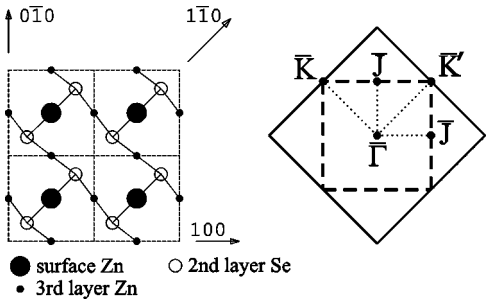

FIG. 11. Left, top view of the ZnSe(001)-$c(2\times2)$ reconstructed surface [four $c(2\times2)$ surface unit cells are shown]. Right, the surface Brillouin zone for this surface. Solid lines show 1×1 and dashed lines $c(2\times2)$ Brillouin zones.

X point induced by surface-Umklapp scattering via $\mathbf{G}_{\mathrm{surf}} = (1,1,0)$ vectors[25] as is apparent from the projected band structure in Fig. 9. The existence of $\mathbf{G}_{\mathrm{surf}} = (1,1,0)$ vectors is a property of the (001) surface of fcc crystals and is independent of the surface reconstruction. The discussed nondispersive features do not arise from the $c(2\times2)$ reconstruction since they were also clearly observed in photoemission spectra from the Se-rich 1×1 surface (not presented here).

V. SURFACE ELECTRONIC STRUCTURE OF ZnSe(001)-$c(2\times2)$

Electronic states at the surface of a single crystal are strictly two-dimensional and have dispersions which differ significantly from bulk states. It is convention to distinguish between surface states which lie in the projected band-gap and surface resonances which lie within the bulk band structure projected on the surface. Surface states can be readily identified using angle-resolved photoemission since they are not mixed with bulk states. If the geometric structure of the atoms in the near surface region is known it is possible to calculate the surface electronic band structure using modern computational techniques. The $c(2\times2)$-reconstruction is the most stable ZnSe(001) surface structure and has been the subject of a number of experimental[8,10,11,13,26,27] and theoretical[28–30] studies. The generally accepted Zn-vacancy model[10] for the ZnSe-$c(2\times2)$ reconstruction was first proposed by Farrell *et al.*[31] Here we compare our ARPES results to *ab initio* theoretical calculations to obtain a more complete understanding of the electronic structure of the ZnSe(001)-$c(2\times2)$ reconstruction.

A. Geometry of the surface

The geometry of the Zn-vacancy model for the $c(2\times2)$ reconstruction and the corresponding surface Brillouin zone are shown in Fig. 11. The relationship between the bulk and surface Brillouin zones is given in Fig. 2. The atomic geometry was established using the FHI98MD program package to minimize the surface energy. The program uses a periodic supercell geometry.[22,32] We used a Zn^{2+} pseudopotential and a slab containing 31 layers (16 layers of Zn and 15 of Se) with $c(2\times2)$ reconstructions on both sides. The vacuum distance between the slabs was equivalent to the thickness of the slab. The relaxation criterium was to minimize the force on each atom below 0.01 eV/Å. The resulting surface energy per $c(2\times2)$ surface unit cell was 1.28 eV lower than for the unrelaxed surface with ideal bulk atomic positions. However, it should be noted that our theoretical relaxed geometry may be slightly inaccurate because the Zn 3*d* states were not included in the pseudopotential. After optimizing the atomic geometry the same slab was used for the band structure calculations.

Several theoretical and experimental results on the geometry of the ZnSe(001)-$c(2\times2)$ reconstruction have been published previously.[10,11,26–30] In Table II we compare our theoretical results to the most recent surface x-ray diffraction measurements.[10] The Zn surface atoms are nearly coplanar with the second layer Se atoms which means that the surface Zn-Se bonds are shorter than the corresponding bulk bonds and the positions of the second layer Se atoms are modified correspondingly.

B. Surface electronic structure of ZnSe(001)-$c(2\times2)$ along $\bar{\Gamma}$-$\bar{J}$

The surface electronic structure of ZnSe(001)-$c(2\times2)$ was established by inspecting the *k*- and eigenvalue-resolved charge densities along the slab. The supercell contained $30\times2=60$ electrons given by the Zn^{2+} and $30\times6=180$ electrons given by the Se^{6+} pseudopotentials. The total number of 240 electrons provides 120 eigenvalues at each *k* point since spin effects are neglected. There are 90 eigenvalues out of these 120 in the valence band between −5 and 0 eV with respect to the VBM. The $\bar{\Gamma}$-$\bar{J}$ distance was sampled in 31 *k* points (including $\bar{\Gamma}$ and $\bar{J}$), and the result is plotted in Fig. 12. In this plot the dots represent the 90 eigenvalues at each *k* point. For each of these eigenvalues the spatial charge density was inspected. The eigenvalue was identified as being surface related and marked with a full circle in Fig. 12 if a significant charge density was located in the surface region

TABLE II. Relative coordinates of the atoms in the ZnSe(001)-$c(2\times2)$ surface reconstruction. The positions are relative to ideal bulk positions and the values are in lattice constant a_0 units using coordinates of the cubic fcc lattice cell. A lattice constant $a_0=5.59$ Å was used for the calculations.

	Position $[a_0]$		
	x (100)	y (010)	z (001)
	Our DFT-LDA results		
Surface Zn	0.000	0.000	−0.199
Second layer Se	0.034	−0.034	0.013
Third layer Zn	0.000	0.000	−0.004
	Weigand *et al.* (Ref. 10) (x-ray data)		
Surface Zn	0.000	0.000	−0.208
Second layer Se	0.029	−0.029	0.010
Third layer Zn	0.000	0.000	0.001
Fourth layer Se	0.003	0.003	0.003
Fifth layer Zn	0.000	0.000	0.004
Sixth layer Se	0.001	−0.001	−0.001

with a small or decaying contribution in the bulk. We found that similar to the calculations on CdTe (Ref. 32) bonding-antibonding combinations of the surface states occur due to artificial interactions across the slab. The surface state between −3.5 and −4 eV exhibits this effect, but the splitting is less than 0.05 eV. We identified three surface-related bands; the two upper bands are localized in the near surface region and the lowest band is more resonancelike and decays over several atomic layers into the bulk.

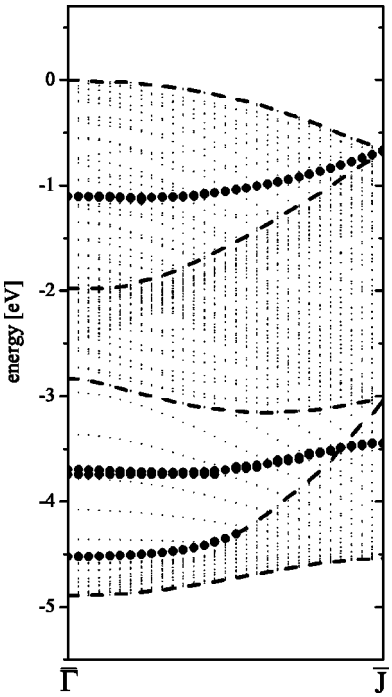

FIG. 12. The eigenvalues from the band structure calculation in the periodic slab geometry. The dots represent the eigenvalues and full circles indicate the eigenvalues for which the charge is located in the surface region (surface states and resonances). The borders of the projected bulk band structure are marked by dashed lines.

The borders of the projected bulk band structure are indicated in Fig. 12. The eigenvalues of the $c(2\times2)$-terminated slab do not correspond exactly to the projected bulk band structure; the projection is folded such that between $\overline{\Gamma}$ and $\overline{J}$ both halves of the bulk Γ-X distance appear due to the supercell of the $c(2\times2)$ reconstruction. The borders of the projected band structure could be easily identified from the density of eigenvalues as indicated in Fig. 12. By comparison with Fig. 13 these borders agree with the projected band structure calculated with the bulk primitive cell geometry.

The use of the Zn^{2+} pseudopotential causes the width of the projected bulk band structure for the *sh* band at X to be reduced to 4.94 eV. The projection of the *sh* band at $X=(1,0,0)\times2\pi/a$ is determined by the dispersion along X-W, and it is only 0.16 eV when calculated with Zn^{12+} including spin effects (as discussed in Sec. IV B), whereas it is 0.44 eV using Zn^{2+}. Our experimental results show that the calculations with Zn^{2+} are more reliable, but Zn^{2+} pseudopotentials are faster and permit larger supercells.

A comparison between the theoretical and experimental results is given in Fig. 13. The above-mentioned splitting of

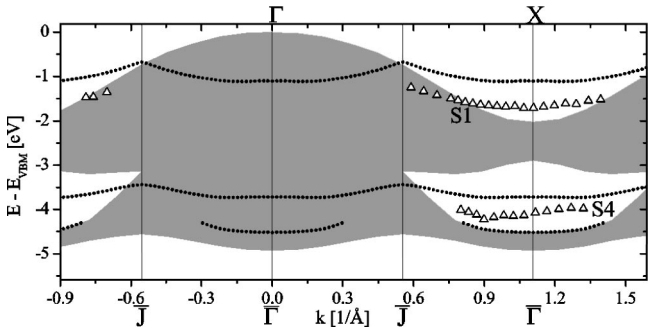

FIG. 13. Surface electronic structure along $\overline{\Gamma}$-$\overline{J}$. Dots show the theoretical calculation and the triangles indicate the same features as in Fig. 7. Shaded areas represent the bulk band structure along [100] projected on the (001) surface.

the theoretical bands due to bonding-antibonding combinations, arising from artificial interaction across the slab, is averaged out and hence is not shown in Fig. 13. The experimental bands are those given in Fig. 7, and we label them S1 and S4 as in Ref. 8. The different periodicity of the projected bulk band structure and surface band structure along $\bar{\Gamma}$-$\bar{J}$ results in surface states only being present in every second period of the $c(2\times2)$ surface Brillouin zone. The energy positions of the calculated surface bands at $\bar{\Gamma}$ are −1.1, −3.7, and −4.5 eV. Both of the surface states S1 and S4 are clearly found in the experimental data, however, the experimental bands are located about 0.4 eV below the calculated positions. This disagreement is related to the Zn^{2+} pseudopotential and is expected from the similar shift of the bulk band structure at *X* for the *lh* band. For S1 and S4 we find good agreement with the results of Xue *et al.*[8]

More surface states were detected in Ref. 8 using the following criteria: (1) when the dispersion could not be assigned to bulk transitions by comparison to the structure plots generated using free electron final states, (2) when the dispersion displayed the same periodicity as the surface BZ, and (3) when the dispersion was insensitive to different excitation energies. As we have shown, an analysis using free-electron final states cannot explain all of the experimentally observed features in the ZnSe(001) spectra, so at least criterium (1) from Ref. 8 is questionable. Criterium (2) can only be applied to the state S1 since the other spectral features showed in Ref. 8 do not extend over enough of the surface BZ. Thus our conclusion is that only surface states S1 and S4 are confirmed experimentally.

The lowest theoretical surface band, a resonance on the edge of the projected bulk band structure, is not found experimentally. However, this is not surprising since this band is not sufficiently localized in the surface region.

The charge densities of the surface bands are shown in Fig. 14 and are similar to the results on CdTe(001)-$c(2\times2)$ given in Ref. 32. It is clear that at $\bar{\Gamma}$ the surface state at −1.1 eV is due to π-like bonding of Se 4*p* states, the surface state at −3.7 eV is due to σ-like bonding of Se 4*p* states, hybridized with Zn 4*s* states, and the resonance at −4.5 eV arises from a combination of π- and σ-like bonds in the surface plane.

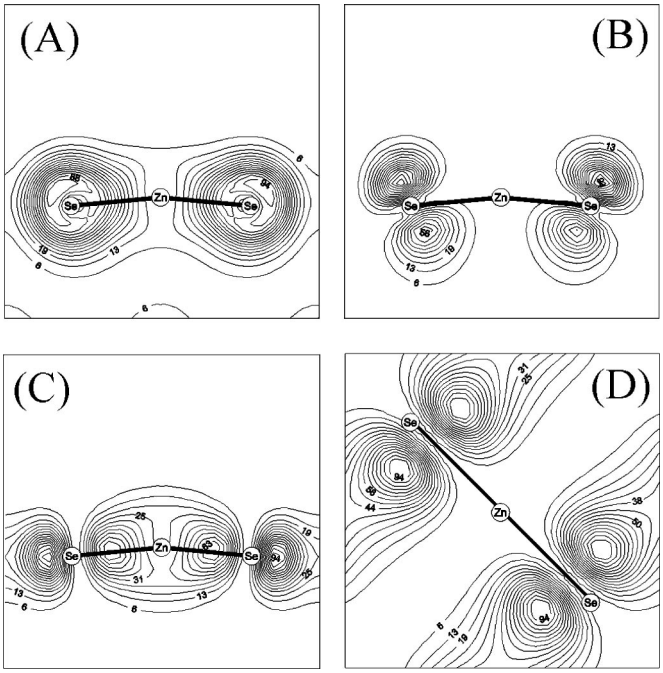

FIG. 14. Charge densities of surface features. (A) Total valence band density of states, (B) dangling-bond surface state at −1.1 eV at $\bar{\Gamma}$, (C) back-bond surface state at −3.7 eV at $\bar{\Gamma}$, and (D) surface resonance at −4.5 at $\bar{\Gamma}$. (A)–(C) are side views in the plane containing the surface Zn atom and second layer Se atoms. (D) is a top view in the plane containing the second layer Se atoms.

VI. CONCLUSIONS

We have performed ARPES measurements on $c(2\times2)$ reconstructed ZnSe(001) epitaxial thin films of thickness 50–100 nm grown on GaAs(001) substrates and compared the spectra to the results of state-of-the-art *ab initio* band structure calculations. The widths of the valence band at the *X* and *L* critical points of the BZ were determined. The experimental final state bands for direct transitions were obtained under the assumption that the theoretical dispersion of the *sh* band is correct. The data analysis in terms of free-electron parabolas and an array of DFT-LDA conduction bands led to the conclusion that the latter can qualitatively explain all of the experimental results.

The surface electronic structure of ZnSe(001)-$c(2\times2)$ was obtained along the $\bar{\Gamma}$-$\bar{J}$ direction. Two surface states were unambiguously identified by comparing the experimental results to the theoretical surface electronic structure and theoretically calculated photoemission spectra. The first surface state is due to dangling bonds originating from Se 4*p* orbitals, and the second is a back-bond surface state arising from the hybridization of Se 4*p* with Zn 4*s* orbitals.

ACKNOWLEDGMENTS

The authors thank the staff of HASYLAB for their assistance. One of the authors (L.P.) would like to thank Stefan Gundel and Kai Rossnagel for helpful discussions. The support of the Deutsche Forschungsgemeinschaft (DFG) through SFB 410 (TP A1, B1, B3, B4), DFG-Graduiertenkolleg 463, and the Bundesministerium für Bildung und Forschung (BMBF) Project 05 KS1GUC/3 is gratefully acknowledged. Calculations were performed at the HLRZ Jülich and at DESY.

*Present address: Department of Physics, Boston University, Boston, Massachusetts 02215. Electronic address: pluto@bu.edu

[1] M. A. Haase, J. Qiu, J. M. DePuydt, and H. Cheng, Appl. Phys. Lett. **59**, 1271 (1991).
[2] D. B. Eason, Z. Yu, W. C. Hughes, W. H. Roland, C. Boney, J. W. Cook, J. F. Schetzina, G. Cantwell, and W. C. Harsch, Appl. Phys. Lett. **66**, 115 (1995).
[3] K. Katayama, H. Matsubara, F. Nakanishi, T. Nakamura, H. Doi, A. Saegusa, T. Mitsui, T. Matsuoka, M. Irikura, T. Takebe, S. Nishine, and T. Shirakawa, J. Cryst. Growth **214/215**, 1064 (2000).
[4] A. Waag, T. Litz, F. Fisher, H.-J. Lugauer, T. Baron, K. Schüll, U. Zehnder, T. Gerhardt, U. Lunz, M. Keim, G. Reuscher, and G. Landwehr, J. Cryst. Growth **184/185**, 1 (1998).
[5] O. Schulz, M. Strassburg, T. Rissom, U. W. Pohl, D. Bimberg, M. Klude, and D. Hommel, Appl. Phys. Lett. **81**, 4916 (2002).
[6] H. Dröge, M. Nagelstrasser, J. Nürnberger, W. Fashinger, A. Fleszar, and H.-P. Steinrück, Surf. Sci. **454–456**, 477 (2000).
[7] Y. Zhang, J. Y. Xue, J. A. C. Foo, A. P. J. Stampfl, D. Wolframm, D. A. Evans, J. D. Riley, R. C. G. Leckey, A. Ziegler, B. Mattern, R. Graupner, M. Hollering, R. Denecke, and L. Ley, Surf. Sci. **377–379**, 288 (1997).
[8] J. Y. Xue, A. P. J. Stampfl, D. Wolfframm, D. A. Evans, M. Hollering, L. Ley, J. D. Riley, and R. C. G. Leckey, Surf. Sci. **401**, L401 (1998).
[9] V. N. Strocov, H. I. Starnberg, P. O. Nilsson, H. E. Brauer, and L. J. Holleboom, Phys. Rev. Lett. **79**, 467 (1997).
[10] W. Weigand, A. Müller, L. Kilian, T. Schallenberg, P. Bach, G. Schmidt, L. Molenkamp, O. Bunk, R. L. Johnson, C. Kumpf, and E. Umbach, Phys. Rev. B **68**, 241314(R) (2003).
[11] W. Weigand, C. Kumpf, M. Sokolowski, A. Bader, C. Schumacher, A. Möginger, W. Faschinger, L. W. Molenkamp, and E. Umbach, Phys. Status Solidi B **229**, 117 (2002).
[12] C. A. Feldmann, R. Engelhardt, T. Permien, E.-E. Koch, and V. Saile, Nucl. Instrum. Methods Phys. Res. **208**, 785 (1983).
[13] W. Chen, A. Kahn, P. Soukiassian, P. S. Magnat, J. Gaines, C. Ponzoni, and D. Olego, Phys. Rev. B **49**, 10 790 (1994).
[14] J. Camassel and D. Auvergne, Phys. Rev. B **12**, 3258 (1975).
[15] S. B. Zhang, S.-H. Wei, and A. Zunger, Phys. Rev. B **52**, 13 975 (1995).
[16] M. Cardona, N. E. Christensen, and G. Fasol, Phys. Rev. B **38**, 1806 (1988).
[17] J. E. Bernard and A. Zunger, Phys. Rev. B **36**, 3199 (1987).
[18] G.-D. Lee, M. H. Lee, and J. Ihm, Phys. Rev. B **52**, 1459 (1995).
[19] O. Zakharov, A. Rubio, X. Blase, M. L. Cohen, and S. G. Louie, Phys. Rev. B **50**, 10 780 (1994).
[20] W. Luo, S. Ismail-Beigi, M. L. Cohen, and S. G. Louie, Phys. Rev. B **66**, 195215 (2002).
[21] M. Nagelstraßer, H. Dröge, H.-P. Steinrück, F. Fischer, T. Litz, A. Waag, G. Landwehr, A. Fleszar, and W. Hanke, Phys. Rev. B **58**, 10 394 (1998).
[22] M. Bockstedte, A. Kley, J. Neugebauer, and M. Scheffler, Comput. Phys. Commun. **107**, 187 (1997).
[23] D. W. Niles and H. Höchst, Phys. Rev. B **43**, 1492 (1991).
[24] D. Olguín, J. A. Rodríguez, and R. Baquero, Eur. Phys. J. B **32**, 119 (2003).
[25] Note, that for fcc material only $\mathbf{G}=(2,2,0)$ and not $\mathbf{G}_{\mathrm{surf}}=(1,1,0)$ is a bulk reciprocal lattice vector.
[26] A. Ohtake, T. Hanada, T. Yasuda, K. Arai, and T. Yao, Phys. Rev. B **60**, 8326 (1999).
[27] Z. Chen, M. Sokolowski, F. Stadler, M. Schneider, R. Fink, and E. Umbach, Europhys. Lett. **59**, 552 (2002).
[28] S. Gundel, Diplomarbeit, Universität Würzburg, 1997.
[29] C. H. Park and D. J. Chadi, Phys. Rev. B **49**, 16 467 (1994).
[30] A. Garcia and J. E. Northrup, J. Vac. Sci. Technol. B **12**, 2678 (1994).
[31] H. H. Farrell, M. C. Tamargo, S. M. Shibli, and Y. Chang, J. Vac. Sci. Technol. B **8**, 884 (1990).
[32] S. Gundel, A. Fleszar, W. Fashinger, and W. Hanke, Phys. Rev. B **59**, 15 261 (1999).